Heritage Science

RESEARCH

Open Access

A study on the characteristics of the excavated pottery in Hanseong and Sabi periods of the Baekje Kingdom (South Korea): mineralogical, chemical and spectroscopic analysis

Hyunkyung Choi[1], Min Su Han[2], Dong Hyeok Moon[3], Chul Sung Kim[4], Sang Won Nam[5] and Young Rang Uhm[1*]

Abstract

The study analyzes the black color factors of black-burnished pottery excavated from the Pungnap Fortress and the Seokchon Tomb during the Hanseong period of the Baekje Kingdom. The current hypothesis surrounding the pottery's black color factors suggests the use of magnetite, manganese oxide, and carbon. To compare the results of the black pottery, red pottery was used as the control group. To identify these black color factors, each hypothesis was investigated using several spectroscopic techniques. However, it was difficult to detect sufficient magnetite and manganese oxide on the surface of the black pottery to account for its black color. In contrast, a larger amount of carbon was located on the surface and core of the black pottery compared to the red pottery. These results indicate that the black factors can be credibly attributed to carbon rather than to magnetite or manganese oxide. The firing temperature of the black-burnished pottery was estimated from the mineral composition based on X-ray diffraction, and the firing atmosphere was deduced from the redox conditions based on the reduction index from Mössbauer spectroscopy. In addition, seven pieces of pottery excavated from Gunsu-ri Temple Site and Buyeo Ancient Tomb from the Sabi period of Baekje were investigated and compared the five pieces of pottery from the Hanseong period. Although the results were based on a limited number of potteries, various firing temperatures and redox atmosphere for pottery from the Hanseong and Sabi periods were carefully proposed.

Keywords Black-burnished pottery, Ceramic, Iron oxide, Amorphous carbon, Mössbauer spectroscopy

*Correspondence:
Young Rang Uhm
uyrang@kaeri.re.kr
Full list of author information is available at the end of the article

Introduction

Baekje, one of the three ancient kingdoms that emerged in the southwestern region of the Korean Peninsula during the Three Kingdoms Period, coexisted with Goguryeo and Silla. The history of Baekje can be divided into three stages—Hanseong (250–475 CE), Ungjin (475–538 CE), and Sabi (538–660 CE) [1, 2]. The earliest stage, the Hanseong period, developed around the Pungnap Fortress, located on the Han River. The Pungnap Fortress (currently located in Seoul, South Korea) is an earthen flatland Fortress situated along the Han River and is presumed to have formed the main Fortress wall of Baekje during the Hanseong period [3, 4]. This site was inhabited by people until the capital was moved to Ungjin (Gongju in South Korea's South Chungcheong Province). Numerous dwellings and water supplies have been identified through excavation surveys within the Fortress, and tens of thousands of ceramics have been unearthed. Types of Baekje pottery include bowls, dishes, plates, tripod bowls/dishes/plates, lids, and pot holders, with the most common types being jars, lids, and lidded vowel [2]. Among the ceramics discovered, pottery has undoubtedly proven the most abundant, with all types of pottery used during the Hanseong period having been found. The fact that a diverse range of pottery types has been excavated from the Pungnap Fortress implies that the Fortress served several functions [5]. This historical site is of paramount importance for clarifying the historical identity of the early Baekje period. Baekje's black-burnished pottery is unique in terms of its shape and technical aspects compared to the pottery of the earlier Three Kingdoms Period [1, 6]. Based on the current findings from pottery excavations, the distribution of black-burnished pottery is almost exclusively concentrated in the central Hanseong region. Black-burnished pottery was primarily excavated from Fortress and Tomb sites in Seoul relating to the Hanseong period of Baekje. One of the ancient tombs where black-burnished pottery was excavated is the ancient tomb in Seokchon-dong, which is located on a low hill in the southeast of central Seoul [7]. The Seokchon-dong Tomb is a stone-built tomb that dates back to the early Baekje period and is presumed to have belonged to the ruling class. Black-burnished pottery has been identified as ware of the social elite, and leaders used it in political gift exchanges to win the loyalty of allies and regional leaders [6, 8]. Therefore, this pottery can be presumed to be the exclusive possession of the Baekje ruling class.

While red (reddish-brown) and grey (greyish-black) pottery have been unearthed throughout the Baekje region, black-burnished pottery has been predominantly excavated from the Pungnap Fortress [9]. Other examples of black-burnished pottery have been discovered in provincial regions dating back to the Hanseong period [10]. Examples include pottery found with only a partially black surface, non-glossy pottery with entirely black surfaces and cores, and non-glossy pottery with black surfaces and non-black cores [10, 11]. However, due to the difficulty of maintaining uniform firing conditions using traditional methods, the color expressed in each part of a pottery may differ. The most prominent features of the black-burnished pottery excavated from the Pungnap Fortress are its highly refined clay body and its black color, distinguishing it from other pottery types.

The factors that produced the black color of this black-burnished pottery have been determined as follows:

i. Magnetite formed by the reduction of iron oxide and oxide-hydroxide. In the case of red pottery, the red color is attributed to hematite (α-Fe_2O_3) and maghemite (γ-Fe_2O_3), whereas in black pottery, the black color (including gray) is attributed to wüstite ($Fe_{1-x}O$), hercynite ($FeAl_2O_4$), and magnetite (Fe_3O_4) [12, 13]. The color development is related to the firing atmosphere. The iron found in the clay turns red to brown in an oxidizing atmosphere and gray to black in a reducing atmosphere [14]. Therefore, the black color of the pottery may be due to reduction firing, which reduces the oxidized iron.
ii. Carbon adsorption from organic matter. The outer surface of the black-burnished pottery has been reported to have a relatively high degree of organic matter [15]. This has been hypothesized as being attributable to the use of colorants derived from the combustion of organic matter. As such, the black color of the black pottery may have been created by the adsorption of carbon derived from the combustion of organic matter (lacquer or plant ash) [2, 16, 17]. Carbon, as a product of the incomplete combustion of fuels when the oxygen supply is insufficient or the proper temperature is not maintained, can appear as black soot on the pottery surface. These fine soot particles can penetrate the surface and the core of the pottery.

Spectroscopic techniques have become standard methods for characterizing the composition of archaeological ceramics [18–20]. Micro-Raman spectroscopy is a technique that obtains qualitative information through non-destructive analysis without sample preparation; thus, determining the pigment composition of a given artifact [21, 22]. The structural characteristics and information on ceramic composition can be obtained using this method. For example, Raman spectroscopy was employed to identify the mineralogical composition of Roma pottery discovered at the Oiasso harbor [23]. The mineral

composition observed from the Raman spectra analysis confirmed that the Roma pottery was fired at high temperatures. Mössbauer spectroscopy allows for the effects of firing on clays to be determined, with the differences originating from various iron compound phases, such as information about the original firing conditions (temperature and atmosphere) [24, 25]. Mössbauer spectra provide hyperfine parameters that can be used to infer the oxidation state and local symmetry of the iron site [26]. Through this method, it is possible to determine the state of iron, such as Fe(II) and Fe(III), in various silicate and oxide phases, depending on the redox conditions during firing [27]. For example, Mössbauer spectroscopy was used when additional information was needed to explain the firing technique of black pottery found in Nepal [28]. Using Mössbauer spectroscopy, the spinel phase and hercynite, which are high-temperature fired minerals, were identified in black slip pottery from Nepal and the firing atmosphere was inferred from the reduction index. The firing atmosphere of pottery can be determined based on the reduction index, defined as the ratio of Fe(II) to total Fe, which can be obtained using the Mössbauer spectroscopy [29]. Furthermore, Mössbauer spectroscopy can be used to identify mineral phases, such as the spinel phase and metallic iron. Notably, Raman and Mössbauer spectroscopy techniques were both employed to analyze the pigments of the Nasca ceramics [14]. Among the various pigments used in Nasca ceramic production, black and red pigments are formed by amorphous carbon and hematite, respectively. X-ray fluorescence spectroscopy and neutron activation analysis provides crucial information for provenance estimation in material analysis by measuring the various major and trace elements present in ceramics [30].

This study investigated the mechanism through which the black color and characteristics of the pottery from the Hanseong period of the Baekje Kingdom were formed, focusing on the black-burnished pottery excavated from the Pungnap Fortress and the Seokchon Tombs. To accurately identify the black color factor of this black-burnished pottery, the surface and core of the pottery were separated and the components of each part were analyzed using various analytical approaches, particularly spectroscopic analysis techniques. In addition, the characteristics of pottery from the Sabi period of Baekje were investigated, and the characteristics of pottery from the early Hanseong period and the late Sabi period of Baekje were compared and analyzed.

Materials and methods

Site and sample information

The Pungnap Fortress is a historic castle site built by the Baekje Kingdom when it established its capital on the Han River (Hanseong period). The excavation of the Pungnap Fortress began in 1997 and is ongoing to this day. Black-burnished pottery from the Hanseong period has been discovered at both the Pungnap Fortress and the Seokchon Tomb sites. Figure 1a shows the locations (Google Maps) of Pungnap-dong and Seokchon-dong in Seoul, South Korea. The present study focuses on the black-burnished pottery excavated from the Pungnap-dong 197 and the Seokchon-dong Tomb and investigates red pottery as a control group for comparison. Among the various pottery pieces analyzed, four representative black-burnished pottery pieces were selected with different colors on the surface and core, and one red pottery piece was selected for comparison. A total of 10 samples were studied by separating the surface and core of each piece of pottery. Table 1 summarizes the data obtained about the black and red pottery pieces taken from the excavation site. "S" and "C" in Table 1 refer to the outer surface and core, respectively.

After the Hanseong and Ungjin periods, the Baekje Kingdom established its capital in Buyeo (Sabi period). Various pottery from the Sabi period was excavated at the Buyeo Gunsuri Temple site and the Buyeo Ancient Tomb (Fig. 1b). Representatively, two soft potteries and five soft-hard potteries were selected, and a total of seven samples were studied. Photographs of the pottery sherds from Fig. 1 is shown in Fig. S1.

Analytical methods

X-ray diffraction (XRD)

XRD patterns of the pottery were obtained to determine the mineral composition and estimate the firing temperature. XRD data were collected using a Rigaku Ultima IV X-ray diffractometer in continuous scanning mode with Ni-filtered Cu-Kα radiation (λ = 1.5406 Å). The working conditions were set at 40 kV and 30 mA, using the ICDD PDF-2 Database. Phase identification was performed using the X'Pert Highscore Plus program in the range of 10–80.

Elemental analyzer (EA)

Elemental analysis was conducted to determine the carbon, hydrogen, and nitrogen compositions of the pottery material. An automatic elemental analyzer (Thermo Fisher Scientific, FLASH 2000) was used with a thermal conductivity detector (TCD). The sample was combusted in a high-temperature furnace, and underwent oxidation and reduction processes. Carbon and hydrogen were converted to carbon dioxide and water, respectively, through combustion, and nitrogen was converted to nitrogen gas. The gas produced was analyzed to determine the ratios of carbon, hydrogen, and nitrogen. Subsequently, the components were detected

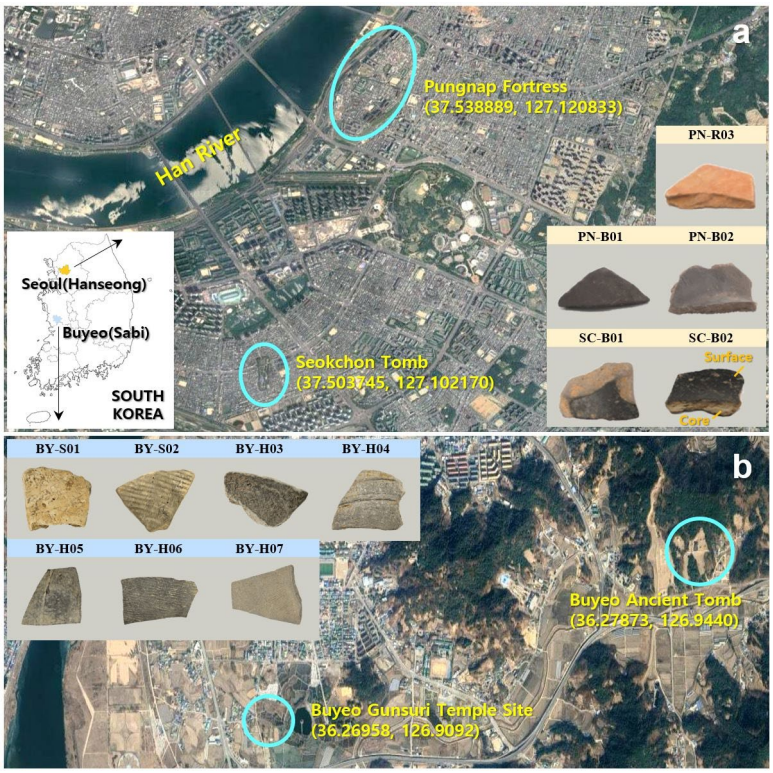

Fig. 1 Map and details of the Pungnap Fortress and the Seokchon Tomb from the Hanseong period, and the Buyeo Ancient Tombs and the Gunsuri Temple site from the Sabi period. Picture of potteries from (**a**) Hanseong (PN-Pungnap, SC-Seokchon) and **b** Sabi period (BY-Buyeo)

Table 1 Samples description with excavation site from the Hanseong and Sabi periods

Hanseong period				
No	**Sample**	**Excavation site**	**Type**	**Color**
1	PN-B01/S	Pungnap Fortress	Black-burnished pottery	Black
2	PN-B01/C	Pungnap Fortress	Black-burnished pottery	Dark grey
3	PN-B02/S	Pungnap Fortress	Black-burnished pottery	Black
4	PN-B02/C	Pungnap Fortress	Black-burnished pottery	Dark brown
5	PN-R03/S	Pungnap Fortress	Red pottery	Yellowish red
6	PN-R03/C	Pungnap Fortress	Red pottery	Light yellowish red
7	SC-B01/S	Seokchon Tomb	Black-burnished pottery	Black
8	SC-B01/C	Seokchon Tomb	Black-burnished pottery	Grayish brown
9	SC-B02/S	Seokchon Tomb	Black-burnished pottery	Black
10	SC-B02/C	Seokchon Tomb	Black-burnished pottery	Grayish brown
Sabi period				
No	**Sample**	**Excavation site**	**Type**	**Hardness**
1	BY-S01	Buyeo Gunsuri Temple Site	Reddish brown pottery	Soft
2	BY-S02	Buyeo Gunsuri Temple Site	Reddish brown pottery	Soft
3	BY-H03	Buyeo Gunsuri Temple Site	Gray pottery	Soft-Hard
4	BY-H04	Buyeo Gunsuri Temple Site	Gray pottery	Soft-Hard
5	BY-H05	Buyeo Gunsuri Temple Site	Gray pottery	Soft-Hard
6	BY-H06	Buyeo Ancient Tomb	Gray pottery	Soft-Hard
7	BY-H07	Buyeo Ancient Tomb	Gray pottery	Soft-Hard

using a TCD. The absolute accuracy of carbon, hydrogen, and nitrogen elements is 0.1 to 0.3%.

Raman spectroscopy

Raman spectroscopy is a well-established technique for characterizing the mineralogical composition of cultural heritage materials, including minerals such as quartz, carbon, and iron oxides. Micro-Raman spectroscopy measurements were performed using a Horiba Jobin Yvon LabRam HR800 instrument with ND: YAG laser excitation (785 nm). The grating was used 600 gr/mm and the spectrum was obtained ranging from 100–2000 cm^{-1} with a resolution of 1 cm^{-1}. The accumulation time was 5 s with three repetitions.

X-ray fluorescence spectroscopy (XRF)

XRF analysis was used to determine the major elements in the pottery samples. XRF was performed using a Rigaku ZSX Primus II spectrometer with a 60 kV, 150 mA (4 kW) Rh anode X-ray tube. The pottery powder was placed inside a polymer holder as a sample. The concentrations of major and trace elements are expressed as percentages, whereas the concentrations of other trace elements are expressed in parts per million (ppm). The relative uncertainty for a given concentration is within 1 to 5% for major elements and exceeds 5 to 10% for some trace elements.

Mössbauer spectroscopy

A transmission-type Mössbauer spectroscopy was performed in a constant acceleration drive at room temperature. A ^{57}Co/Rh source of nominal strength 50 mCi was used as γ-source. The γ-ray detector used a beryllium side window proportional counter filled with Xe gas. The Mössbauer spectra were recorded with a 512-channel spectrometer and the velocity range was set to ±12 mm/s. The pottery powder was prepared by dispersing it in a 2 cm diameter sample holder. Isomer shift data are presented relative to those of metallic α-Fe. The hyperfine parameters of the spectra were fitted to the Lorentzian line shapes using the standard least-squares method. The unit of the isomer shift (IS), quadrupole splitting (QS), and full line width at half maximum (Γ) is expressed in mm/s. The proportion of each Fe species is proportional to the relative spectral area. Different types of Mössbauer spectra that can be associated with different firing procedures have been defined, primarily based on the positions and intensities of components in the Mössbauer spectrum [14].

Results and discussion

Black-burnished pottery from the Hanseong period: black color development

Mineralogical composition

Most clay pottery exhibits differences in color, hardness, and other properties owing to variations in temperature, atmosphere, and duration of the firing process. The temperature range at which pottery is fired can be known through XRD due to changes in minerals that occur during the process of making pottery [31]. When clay minerals are fired at high temperatures, it includes components, such as silica (SiO_2) that melt and vitrify, making the pottery much harder. The crystal structure of clay minerals begins to change at temperatures above 500 °C. When the temperature exceeds 900 °C, the original structure transforms into new silicate minerals. Figure 2a shows the XRD pattern of the pottery, where quartz, plagioclase, orthoclase, and mica were commonly observed on the surface and core of all the analyzed samples. XRD analysis showed no significant difference in the mineral composition between the surface and core of

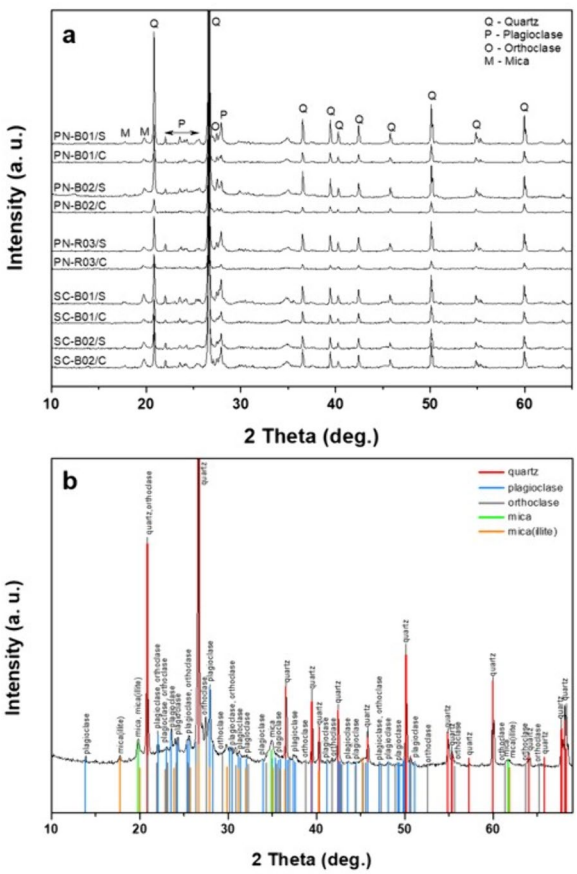

Fig. 2 **a** XRD patterns of black-burnished and red pottery from the Hanseong period. **b** XRD patterns of PN-B01/S and references of minerals

the pottery. In general, pottery contains minerals, such as quartz, feldspar, and mica, allowing for the estimation of the firing temperature. The raw pottery materials undergo phase transitions or decompose into different minerals as the firing temperature increases. Illite, begins to decompose when the firing temperature exceeds 900 °C, and feldspar decomposes at temperatures above 1200 °C. Based on the XRD pattern observed in pottery in which mullite were not observed and feldspar and illite remained, the firing temperature of Hanseong pottery was estimated to be below 900 °C. The color of pottery is closely related to the composition of the raw clay; however, it is greatly influenced by the firing atmosphere. This refers to whether oxygen is continuously supplied or not during the firing process, and whether this firing atmosphere is related to iron oxide. When pottery is fired with a continuous supply of oxygen, the iron in the clay is oxidized, giving the pottery a reddish color. Conversely, if the oxygen supply is blocked, a reduction reaction occurs, resulting in dark colors, such as gray or black. Figure 2b shows the results obtained from matching the black-burnished pottery (PN-B01/S) with the reference data of minerals. Major minerals contain quartz, plagioclase, orthoclase, and mica. In addition, it is expected that iron oxide minerals, such as hematite, maghemite, and magnetite, remain present in the pottery. Figure S2 shows the comparison of the representative black (PN-B01) and red (PN-R03) pottery with reference data of iron oxide and oxide-hydroxides. However, it is difficult to confirm the level of iron oxide peaks due to the relatively high peaks of quartz and feldspar.

Geochemical features

The pottery samples taken from the Pungnap-dong and Seokchon-dong archaeological sites, both major and trace elements were analyzed. The geochemical features of the pottery samples obtained through XRF are listed in Table 2. The major elements found in the pottery samples include SiO_2 and Al_2O_3. The black-burnished pottery excavated from the Pungnap Fortress and the Seokchon Tomb shows a SiO_2 content ranging from 61.86–64.52wt% and an Al_2O_3 content ranging from 19.66–23.26wt%. The content of Fe_2O_3 in red pottery is 8.34–8.82wt%, whereas it is relatively low in black-burnished pottery, ranging from 3.50–5.62wt%. This suggests that Fe_2O_3, which was assumed to be highly related to the black color expression, was not present in a higher proportion in the black-burnished pottery samples than in the red pottery. In addition, while Fe_2O_3 can be present in the clay used as a raw material, these minerals can appear as by-products created during the firing process as the iron-bearing minerals in the raw material are destroyed and recrystallized [32]. The CaO content in the black-burnished pottery samples obtained from the Pungnap Fortress is 0.88–1.02wt%, which is slightly higher than the black-burnished pottery samples taken from the Seokchon Tomb (0.70–0.77wt%). CaO is abundant in plant ash [33], and P_2O_5 is presumed to be generated in the process of burning plants and coating them with soot [34]. The difference in the CaO content between black and red pottery is presented in Fig. 3. Similarly, the P_2O_5 content in black-burnished pottery was found to be more than 1wt%, whereas it was less than 1wt% in the red pottery control samples. The contents of black-burnished pottery have 0.94–1.15wt% of MgO, 0.95–1.45wt% of TiO_2, 0.60–0.98wt% of Na_2O, and 2.33–2.96wt% of K_2O. Phyllosilicates are a group of silicate minerals named for their layered atomic arrangements. K and Ca are related to illite, whereas Mg and Al reflect the presence of phyllosilicates [35].

Black color component

Black-burnished pottery has been reported to be influenced by organic elements, such as carbon and hydrogen

Table 2 Major elements (wt%) and trace elements (ppm) of pottery obtained by XRF

Sample	SiO_2	Al_2O_3	MgO	Na_2O	K_2O	CaO	Fe_2O_3	TiO_2	P_2O_5	MnO	Ba	Sn	Ni	V	Zr	Cr	Zn	Sr	Rb	Cu
PN-B01/S	64.52	20.80	1.04	0.71	2.96	1.02	4.58	1.45	2.41	< 0.05	2101	355	170	152	156	290	140	140	140	109
PN-B01/C	64.21	21.85	1.01	0.69	2.88	0.92	4.24	1.37	2.24	< 0.05	1925	496	219	147	150	331	123	127	125	47
PN-B02/S	63.11	22.53	1.15	0.61	2.38	0.95	4.88	1.40	1.92	< 0.05	1345	451	193	200	136	267	113	128	142	112
PN-B02/C	61.86	23.26	1.11	0.60	2.35	0.88	5.62	1.37	1.81	< 0.05	1846	426	190	283	203	286	163	114	174	32
PN-R03/S	59.72	24.10	0.79	0.56	2.91	0.48	8.82	1.47	0.41	< 0.05	1496	241	196	105	197	393	111	202	148	59
PN-R03/C	58.76	23.24	0.76	0.52	2.99	0.39	8.34	1.51	0.44	< 0.05	1244	245	144	95	364	382	184	146	125	77
SC-B01/S	64.03	20.73	1.05	0.93	2.60	0.77	4.65	0.99	2.03	< 0.05	1192	298	195	140	168	228	116	121	121	109
SC-B01/C	62.84	21.41	0.99	0.97	2.41	0.73	5.21	1.05	1.85	< 0.05	1074	358	205	146	151	195	111	133	132	72
SC-B02/S	63.12	20.52	1.07	0.93	2.56	0.75	3.50	1.03	2.03	< 0.05	1083	346	201	168	146	231	109	94	126	106
SC-B02/C	62.72	19.66	0.94	0.98	2.33	0.70	4.07	0.95	1.97	< 0.05	1124	343	194	209	199	206	140	128	118	57

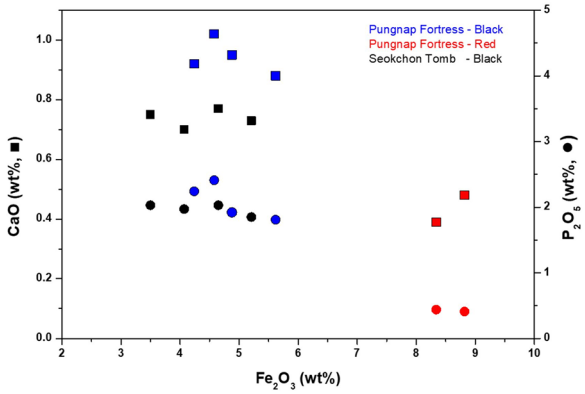

Fig. 3 Distribution diagram showing CaO and P_2O_5 vs. Fe_2O_3 of potteries

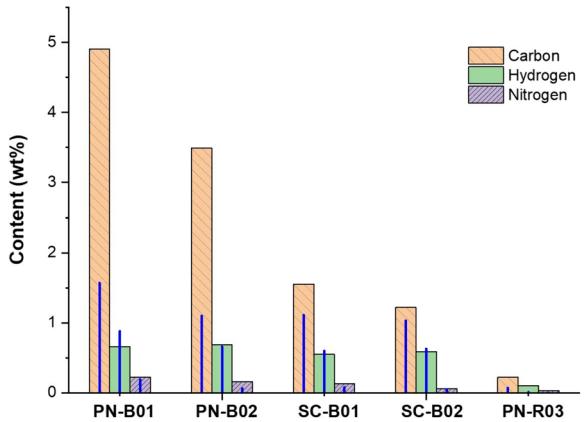

Fig. 4 EA result of the organic matter in the pottery samples from the Pungnap Fortress and the Seokchon Tomb (Bar is surface and drop line is core)

[36]. Therefore, to quantify the total amount of carbon in the black-burnished pottery samples used in this study, an EA measurement was conducted. The carbon, hydrogen, and nitrogen contents of the organic elements analyzed are presented in Fig. 4. A carbon content of over 1wt% was found in all black-burnished pottery, excluding red pottery (PN-R03). In particular, the carbon content of PN-B01/S has a maximum value of 4.91wt%. Among the measured organic elements, the nitrogen content was low in general; however, it was at its highest, at 0.22wt%, in PN-B01/S. Furthermore, the black-burnished pottery excavated from the Pungnap Fortress site showed relatively higher carbon content compared to the samples found at the Seokchon Tomb site. It was confirmed that the carbon content of the black-burnished pottery excavated from the Pungnap Fortress was high both on the surface and in the core, which can be explained by the penetration of the black material from the surface to the core. This is similar to one of the results obtained by observing the cross-section of black-burnished pottery with optical and polarizing microscopes. According to the reported results [36], the cross-section of the pottery was divided into two types; the type with deeply fade cross-section from the surface to the depth and the other is that a fine, thin black layer is observed on the surface. Hence, it can be inferred that the black material in black-burnished pottery is more closely related to the presence of carbon rather than magnetite, supporting previous studies [14, 36–38]. For example, microscopic observations and Raman spectroscopy measurements of black pottery from the Bronze Age in Denmark revealed that the black material in the pottery was tar obtained from birch [37]. Furthermore, using Raman spectroscopy and XRF, it was discovered that the observed black coating on pottery pigment, dating from the sixth century BCE found in Keeladi, India, was formed of carbon nanotubes [38]. In addition, based on the results obtained from the Time-of-Flight Secondary Ion Mass Spectrometry (ToF–SIMS measurements), the black material of the black pottery was composed of urushiol, the main component of lacquer [36].

Several researchers use Raman spectroscopy to complement XRD and XRF information [39]. Amorphous carbon peaks were not observed in the XRD patterns of the pottery because of the presence of high peaks of quartz and feldspar. However, since a high carbon content was determined from the EA measurements, it can be assumed that carbon was present in the pottery. The Raman spectra of the black-burnished pottery excavated from the Pungnap Fortress site and the Seokchon Tomb site are presented in Fig. 5. The Raman bands (462 cm^{-1} [40, 41]) appearing on the surface and core of the black pottery indicate the presence of quartz. As shown in Fig. 5, some of the Raman bands of quartz appear very broad. The bands become broader as the firing process distorts the crystalline structure of quartz [42]. If the Raman bands of quartz exist in free or isolated forms, such as SiO_2, they appear very intense and narrow [43]. Therefore, the changes in the morphology and structure of quartz can be evaluated based on the intensity and shape of the Raman bands. The presence of Illite shows a band at approximately 707 cm^{-1} [44]. In Fig. 5, the Raman bands cannot distinguish the presence of illite. This is because Raman signals are weak, and the Raman peaks are often obscured by noise. The measured Raman spectra showed a broad band and a strong fluorescence background for the pottery samples. This made it difficult to distinguish between the Raman bands of feldspar (plagioclase and orthoclase). The broadening of the Raman bands around 1357–1360 cm^{-1} and 1585–1595 cm^{-1} can be explained by the presence of amorphous carbon [45, 46]. Raman bands corresponding to amorphous carbon

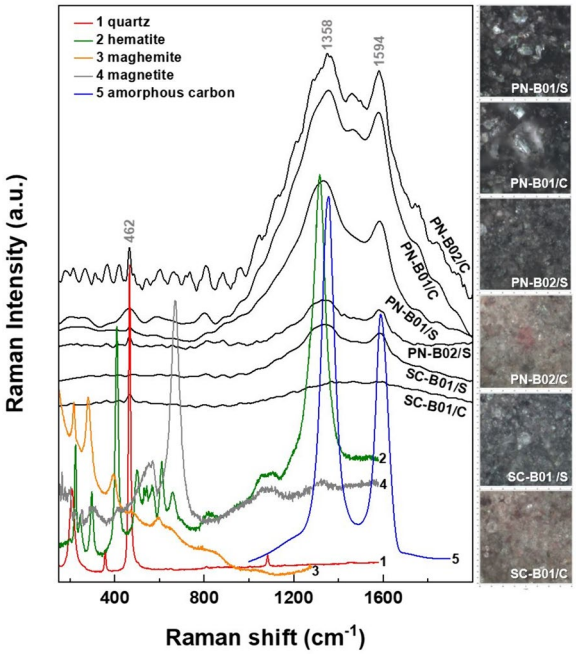

Fig. 5 Micro Raman spectra obtained from PN-B01/S, PN-B01/C, PN-B02/S, PN-B02/C, SC-B01/S, and SC-B01/C. Reference spectra (Figure legend) are provided for comparison with the spectra of samples

were confirmed on the surface and core of the black-burnished pottery. Plant ash or urushiol (the main components of lacquer) may be considered as sources of carbon.

To solve the fluorescence problem in the samples, the pottery samples were measured using FT-Raman spectroscopy (Nd:YAG laser with a wavelength of 1064 nm). However, satisfactory data could not be obtained.

How to characterize Fe-based minerals in pottery

From the XRD results, the crystalline phase composition of the pottery can be identified, which provides information for investigating the raw materials and firing techniques used in pottery creation. Through XRD, only the crystalline compositions of quartz and feldspar (both plagioclase and orthoclase) were identified in the pottery, whereas metal oxides and other phases were not found because of their low content and amorphous nature. In the case of amorphous carbon, it was confirmed using Raman spectroscopy; however, the presence of iron oxide, which is most abundant in soil, could not be confirmed. The firing effect on clays can be studied by tracking the transformation of the components of the Mössbauer spectrum with different iron-containing phases. ^{57}Fe Mössbauer studies can be combined with other techniques such as XRD, mineralogical, and geochemical analysis to help gather information about how pottery was produced.

The Mössbauer spectra of the black-burnished pottery (B-PN, B-SC) are presented in Fig. 6. The pottery spectrum consists of only doublets. In many ancient pottery works, sextets have been found in the room-temperature Mössbauer spectrum [14, 47–49]. However, unlike other

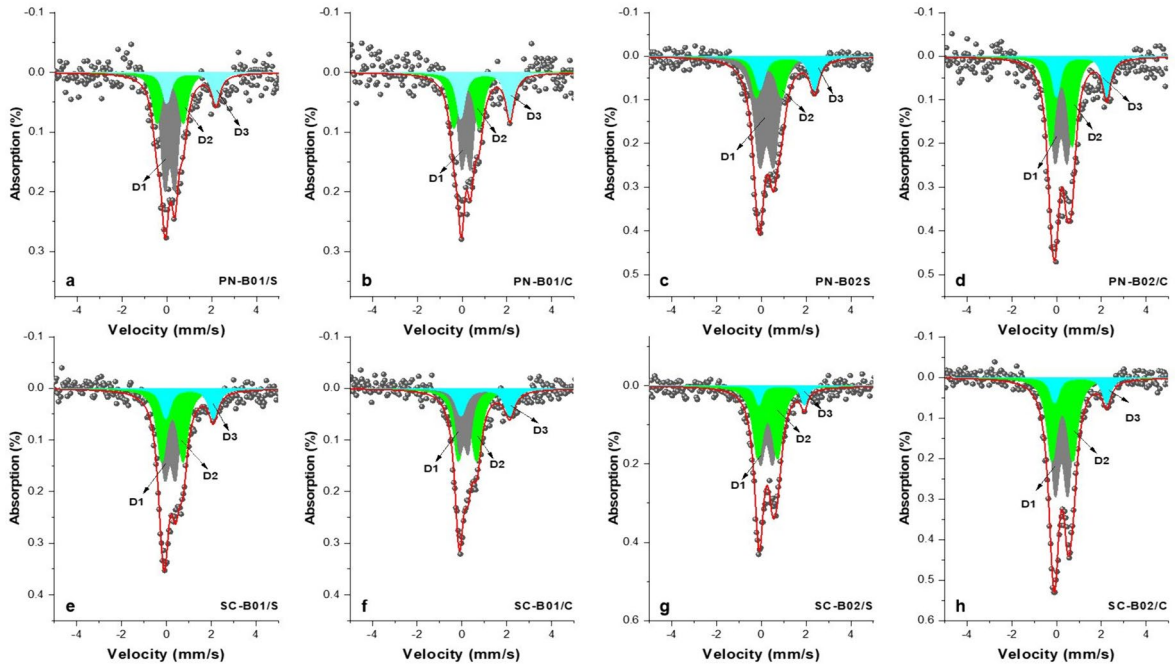

Fig. 6 Mössbauer spectra of black-burnished pottery (**a**–**h**); PN-B01/S, PN-B01/C, PN-B02/S, PN-B02/C, SC-B01/S, SC-B01/C, SC-B02/S, and SC-B02/C

types of pottery, the pottery used in this study does not contain a sextet of hematite, magnetite, or goethite. All the spectra showed strong paramagnetic Fe(III) absorption and weak Fe(II) absorption. From a, c, e, and g in Fig. 6, the surface of the black-burnished pottery was analyzed as D1 and D2 corresponding to Fe(III), and D3, corresponding to Fe(II). The D1 and D2 doublets are associated with the presence of nanosized iron oxide particles and Fe(III)-bearing silicates. Nanosized oxide and/or oxyhydroxide particles exhibit superparamagnetic behavior as doublets at room temperature [50, 51]. Superparamagnetic doublets are difficult to distinguish between minerals at room temperature. The types of magnetically ordered species can be described by low temperature measurements. The observed D3 parameter (IS = 0.94–1.15 mm/s, QS = 2.08–2.35 mm/s) arises from the paramagnetic Fe(II) ions present in the Fe(II)-bearing silicate [28, 52, 53]. The low ratio of Fe(II) to the silicate sub-spectrum demonstrates that the pottery was fired under controlled oxidizing conditions. The firing conditions, firing temperature, and color mechanism of archaeological pottery can be inferred based on the presence or absence of paramagnetic Fe(II) and Fe(III) ions.

Figure S3 shows the Mössbauer spectra of the red pottery (PN-R03). Similarly, no other sextet spectrum was found in the red pottery. The line width of the site for each spectrum may vary due to the overlapping of iron oxides and/or oxyhydroxides, poor crystallinity, and small particle size. The fitted Mössbauer parameters are listed in Table S3.

Reddish brown and gray pottery from the Sabi period: hardness and firing temperature

Mineralogical composition

XRD analysis was conducted to determine the mineral composition of the Sabi period potteries and estimate the firing temperature (Fig. 7). The main minerals of pottery are quartz, feldspar, and mica. In some pottery, mica, mullite, hercynite, and hematite, which indicate high firing temperatures, were detected differently, therefore, it is assumed that the Sabi period pottery was sintered at various firing temperatures. The differences in the mineralogy of potteries lead to three groups:

- Mineralogical Group 1: Quartz + Feldspar (Plagioclase and Orthoclase) + Mica; BY-S01, BY-S02
- Mineralogical Group 2: Quartz + Feldspar (Plagioclase and Orthoclase); BY-H03, BY-H04
- Mineralogical Group 3: Quartz + Feldspar (Plagioclase and Orthoclase) + Mullite + Hematite or Hercynite; BY-H05, BY-H06, BY-H07

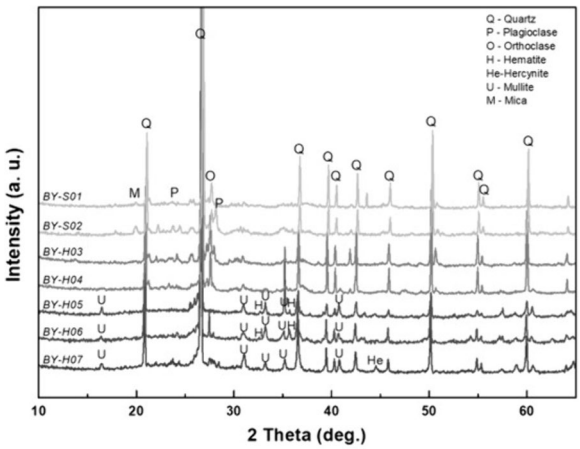

Fig. 7 XRD patterns of the potteries from the Sabi period

The firing temperature for pottery in groups 1, 2, and 3 is as follows: Group 1 is fired below 900 °C, resulting in soft pottery; Group 2 is sintered at 900–1000 °C, yielding soft-hard pottery; and Group 3 is sintered at 1000–1100 °C, also producing soft-hard pottery. These temperature ranges are determined based on the detection of high-temperature fired minerals. Additionally, Group 1 shares the main mineral composition with Hanseong period pottery.

In group 2, the mica peak disappeared, therefore, the potteries were fired at a temperature above 900 °C. In group 3, hematite is detected in the pottery of BY-H05 and BY-H06. This has a reddish-brown cross-section and is presumed to have been formed without sufficient experience in a reducing atmosphere. Depending on the firing temperature, group 1 was confirmed as soft, group 2 and 3 as soft-hard.

Geochemical features

The major elements of the Sabi period pottery were analyzed (Table S2). In general, the major elements of clay are SiO_2 and Al_2O_3, which maintain viscosity and facilitate molding. Quartz, one of the main raw materials for pottery, has a high melting point and maintains the shape of ceramics. In addition, feldspar, one of the main raw materials of clay, plays a flux role in the firing process as the viscosity and firing temperature of the clay is determined by the content of feldspar [54]. The results of the XRF analysis of pottery from the Hanseong and Sabi periods of Baekje are compared in Fig. 8. Clay minerals are decomposed into SiO_2 and Al_2O_3 during the firing process to produce mullite at high temperatures. The liberated SiO_2 components remain after being converted to quartz, tridymite, or cristobalite. Mullite ($3Al_2O_3{\cdot}2SiO_2$) is a crystal phase that is easily formed as the Al_2O_3

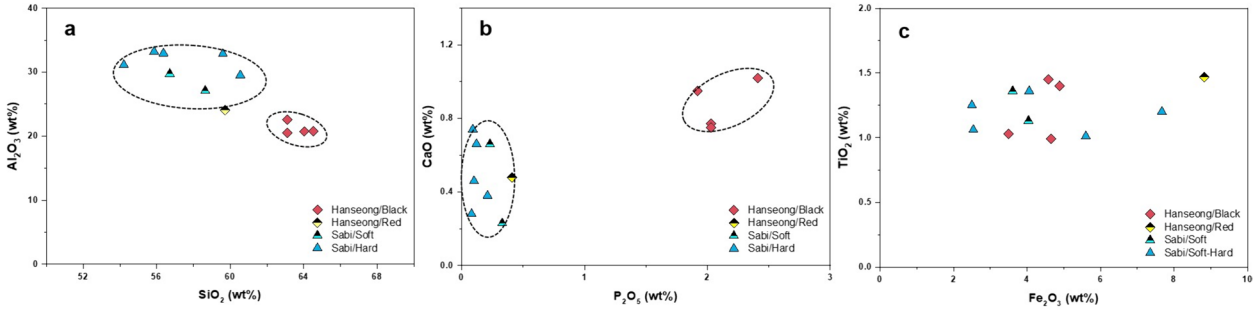

Fig. 8 Scatterplots of **a** SiO_2–Al_2O_3, **b** P_2O_5–CaO, and **c** Fe_2O_3–TiO_2 of the Hanseong and Sabi period potteries

content increases [55]. The SiO_2-Al_2O_3 distribution diagram for this is presented in Fig. 8a. From the high Al_2O_3 content of the Sabi period pottery, it can be inferred that it was fired at a temperature of over 1000 °C or was fired for a long duration. The CaO content of Sabi pottery was 0.28–0.77 wt%, which was lower than the Hanseong pottery. In particular, the P_2O_5 of Sabi pottery was 0.10–0.33 wt% (Hanseong pottery: 0.41–2.41 wt%), showing a clear difference (Fig. 8b). The content distribution of the coloring components, Fe_2O_3 and TiO_2, are presented in Fig. 8c. The TiO_2 content is maintained at 1.0–1.5wt%, regardless of the production period, and the Fe_2O_3 content is almost similar.

How to determine the firing atmosphere of pottery

The Mössbauer spectra of the pottery from the Sabi period are presented in Fig. 9. To understand the firing atmosphere of pottery from the Hanseong and Sabi periods of Baekje, it was estimated through the iron compounds from the Mössbauer results. The Mössbauer spectra of soft and soft-hard pottery consist only of doublets (Fig. 9a–d). Soft potteries of group 1 are similar to the spectrum of pottery from the Hanseong period. The D4 site, corresponding to the Fe(II) state in soft-hard pottery (group 2), increased relative to that of soft pottery (group 1). The spectra of soft-hard pottery (BY-H05 and BY-H06 of group 3) were analyzed with sextet of

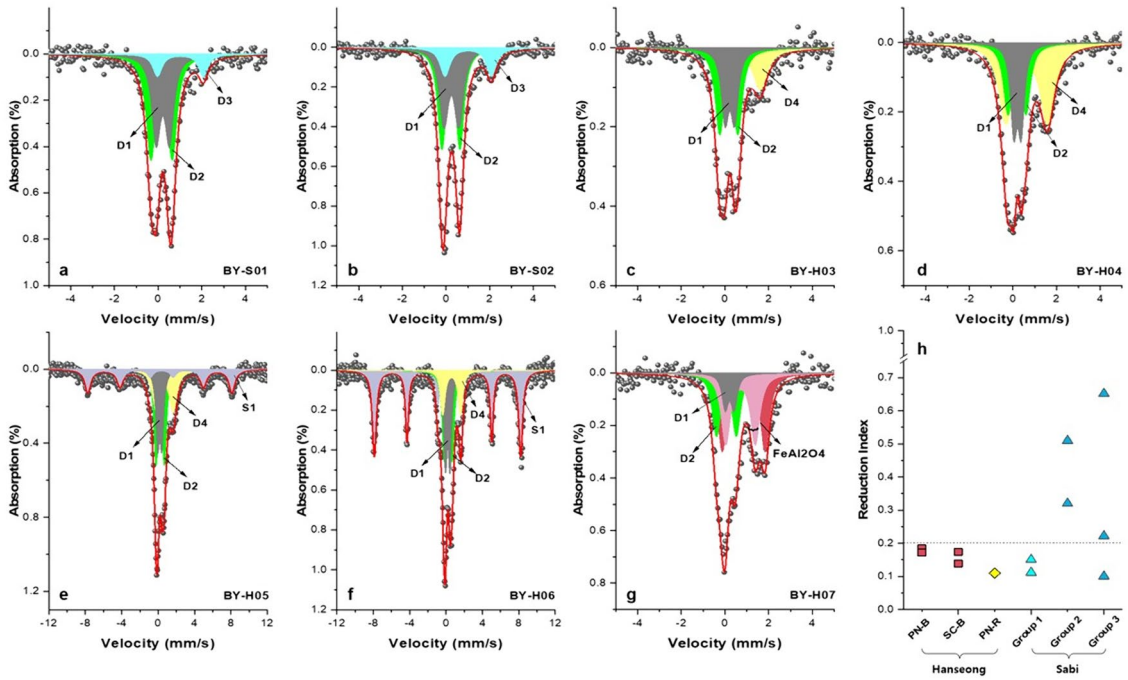

Fig. 9 Mössbauer spectra of the potteries (**a**–**g**); BY-S01, BY-S02, BY-H03, BY-H04, BY-H05, BY-H06, and BY-H07. **h** Reduction index of the potteries from the Hanseong and Sabi periods

hematite and three doublets (Fig. 9e–f). Considering that mullite was confirmed in XRD, it is presumed that these two potteries (BY-H05 and BY-H06) were fired at high temperatures; however, hematite confirms that they were not sufficiently fired in a reducing atmosphere. The other pottery (BY-H07 of group 3) was analyzed as D1, D2, and hercynite ($FeAl_2O_4$). When the biotite, vermiculite, and chlorite containing Fe collapse at high temperatures and then Fe combines with Al, the hercynite is formed at 900–1000 °C. In hercynite, Fe(II) ions occupy both tetrahedral (T_d) and octahedral (O_h) sites [56, 57]. The presence of Fe(II) means that the ceramics were likely produced in a reducing atmosphere. Hercynite has Fe(II) ion state and is black in color. However, in the color analysis of pottery, if the pottery is gray, it may be the result of a reducing atmosphere or insufficient oxidation of the carbon component in the clay.

Although it is difficult to distinguish sites among clay minerals from the Mössbauer spectra, the relative amounts of Fe(II) can serve as a basis for comparison with the reduction index (RI) of archaeological pottery to understand their firing atmosphere [27, 28]. According to previous research [29, 58–60], the atmosphere in which pottery is fired can be deduced from the RI. The RI is calculated from the Fe(II) area of the Mössbauer spectrum and represents the contribution of reduced iron to total iron ($Fe(II)/Fe_{tot}$). RI values greater than 0.20 relate to reducing conditions, whereas RI values less than 0.20 indicate oxidizing conditions. Figure 9h was plotted against the RI values to identify possible clustering among the Hanseong and Sabi periods. The RI value of 0.20, indicated by the dashed line in the graph, represents the upper limit of amount of Fe(II) in the analyzed clays. The RI values of Hanseong period potteries and Sabi period soft potteries (group 1) less than 0.20, indicating that the potteries were fired in an oxidizing atmosphere. However, it is presumed that the black-burnished pottery from the Hanseong period went through a reducing atmosphere process in which carbon was absorbed by closing the kiln in the final firing stage. The RI values of group 2 and BY-G07 of group 3 are greater than 0.2, and the presence of high Fe(II) indicates that they were calcined in a reducing atmosphere. It can be assumed that the hematite in BY-H05 and BY-H06 was fired in an incomplete oxidation/reduction atmosphere.

Conclusion

The purpose of this study is to characterize the color and firing conditions of black-burnished and red pottery samples dating from the Hanseong period of the Baekje Kingdom and investigate the characteristics of pottery from the Sabi period of Baekje. Various spectroscopic methods (X-ray fluorescence, Raman, and Mössbauer spectroscopy), XRD, and EA measurements were used to evaluate the black color factor and firing temperature of the black-burnished pottery. In this study, the mineralogy and physical properties of black-burnished and red pottery samples excavated from the Pungnap Fortress and the Seokchon Tomb sites were analyzed. The presence of mica in all measured pottery samples indicated the firing temperature to be below 900 °C. Based on the reduction index, the firing conditions of these pottery samples indicate that they took place in a controlled oxidizing atmosphere, which includes reduction atmosphere processes. The black color factors of black-burnished pottery are presumed to be due to carbon, rather than iron oxides. The basis for this is the high carbon content in EA measurement, the higher CaO and P_2O_5 contents in XRF than in red pottery, no crystalline carbon peak observed in XRD, rather an amorphous carbon peak measured in the Raman band, and magnetite of sextet not observed in the Mössbauer spectrum (the nanocrystalline phase may exist; however, the amount present in the pottery samples was insufficient to be considered a factor in the black color). Based on these results, it is probable that the black color factor in black pottery can be attributed to amorphous carbon.

The characteristics of the Sabi period pottery were analyzed according to firing temperature and hardness. Hardness increases as the firing temperature increases and the firing temperature was confirmed by high-temperature calcination minerals (mullite and hercynite) through XRD patterns. As a result of the Mössbauer analysis, the Fe(III) content of group 1 (soft pottery) was higher than the Fe(II) content, and the Fe(II) content of groups 2 and 3 (except hematite) was relatively higher than the Fe(III) content. Therefore, this suggests that the Sabi period pottery was produced at a more diverse firing temperature and atmosphere than the Hanseong period pottery.

Five pieces of pottery from the Hanseong period of Baekje and seven pieces of pottery from the Sabi period were analyzed and compared, and the results are limited by focusing on a limited number of potteries. Therefore, in order to obtain additional information about the firing technology of Baekje pottery, additional research must be conducted on pottery of many different colors. Another potential approach would involve the manufacture of suitable fired clay and ceramic samples that could be used to facilitate further investigations.

Abbreviations

XRD	X-ray diffraction
TCD	Thermal conductivity detector
ppm	Parts per million
XRF	X-ray fluorescence spectroscopy
EA	Elemental analyzer
IS	Isomer shift

QS Quadrupole splitting
RI Reduction index

Supplementary Information

The online version contains supplementary material available at https://doi.org/10.1186/s40494-024-01336-9.

Additional file 1: Table S1. Mineral compositions and firing temperature of the potteries from the Hanseong and Sabi periods of the Baekje Kingdom. Table S2. Major elements content (wt%) of the potteries from the Sabi period. Table S3. Mössbauer parameters for black-burnished and red pottery from the Hanseong period. Table S4. Mössbauer parameters for the potteries from the Sabi period. Figure S1. Photographs of the studied samples. Figure S2. XRD patterns of PN-B01 and PN-R03 with references (Iron oxide; wüstite, magnetite, hematite, and maghemite. Iron oxide-hydroxides; goethite, lepidocrocite, akageneite, feroxyhyte, ferrihydrite, and bernalite). Figure S3. Mössbauer spectra of red pottery; PN-R03/C and PN-R03/C.

Acknowledgements
The authors would like to thank the Korea National University of Cultural Heritage and Buyeo National Research Institute of Cultural Heritage for providing the samples.

Author contributions
HC performed all experiments, and analyzed all datasets and figures and interpretation of the analytical data as well as preparing and editing the manuscript; MSH and SWN prepared the archaeological data of the site and samples and also contributed to sampling; DHM and CSK collected data and analyzed all datasets; YRU reviewed the manuscript, acquired funds, and supervised the overall project. All authors read and approved the final manuscript.

Funding
This work was supported by the National Research Foundation of Korea (NRF) grant fund from the Korean government (MSIT) (No. NRF-2022R1A2C2092277).

Availability of data and materials
The datasets used and/or analyzed during the current study are available from the corresponding author on reasonable request.

Declarations

Competing interests
The authors declare that they have no competing interests.

Author details
[1]HANARO Utilization Division, Korea Atomic Energy Research Institute, Daejeon 34057, Republic of Korea. [2]Department of Heritage Conservation and Restoration, Graduate School of Cultural Heritage, Korea National University of Cultural Heritage, Buyeo 33115, Republic of Korea. [3]Geological Museum, Korea Institute of Geoscience and Mineral Resources, Daejeon 34132, Republic of Korea. [4]Department of Physics, Kookmin University, Seoul 02707, Republic of Korea. [5]Cultural Heritage Administration, Daejeon 35208, Republic of Korea.

Received: 13 February 2024 Accepted: 22 June 2024
Published online: 09 July 2024

References

1. Kim M, Shin HN, Kim J, Roh KJ, Ryu A, Won H, et al. The ins and the outs: foodways, feasts, and social differentiation in the Baekje Kingdom, Korea. J Anthropol Archaeol. 2016;43:128–39. https://doi.org/10.1016/j.jaa.2016.07.014.
2. Blackmore H, Cho D, Lee H-W. All for one? The production of black burnished pottery and state formation in the early Korean polity of Baekje. Archaeometry. 2021;63(3):531–48. https://doi.org/10.1111/arcm.12632.
3. Park S. The beginning and the end of Baekje capital. Jungang Gogo Yeongu. 2013;13:1–34.
4. Kim M. Leadership in the Emergent Baekje State: state formation in Central-Western Korea (ca. 200–400 CE). Open Archaeol. 2023;9(1):20220313. https://doi.org/10.1515/opar-2022-0313.
5. Choi J. The development of the pottery technologies of the Korean peninsula and their relationship to neighboring regions. In: Byington ME, editor. Early Korea1. Cambridge: Korea Institute, Havard University; 2008. p. 157–98.
6. Park SB. The study on the emergence of Baekje pottery style. Baekje Study. 1992;23:21–64.
7. Kwon OY, Byington M. Early Korea 1: reconsidering early korean history through archaeology. Early Korea Project. Korea Institute, Havard University, Seoul; 2008. p. 65–112.
8. Park SB. A study of the state formation of Paekche. Seoul: Seogyeong Munhwasa; 2001.
9. Nam SW. As production technology, the meaning of the black burnished pottery in Baekje Dynasty. J Kor Archaeol. 2013;89:94–137.
10. Nam SW. A study of black burnished pottery in Beakje dynasty. Master's thesis Chungbuk National University. 2013.
11. Lee NS. An examination of black burnished pots in Baekje dynasty. Prehistory and Ancient History. 2001;16:177–99.
12. Ménager M, Esquivel PF, Conejo PS. The use of FT-IR spectroscopy and SEM/EDS characterization of slips and pigments to determine the provenances of archaeological ceramics: the case of Guanacaste ceramics (Costa Rica). Microchem J. 2021;162: 105838. https://doi.org/10.1016/j.microc.2020.105838.
13. Aloupi-Siotis E. Ceramic technology: how to characterise black Fe-based glass-ceramic coatings. Archaeol Anthropol Sci. 2020;12(8):191. https://doi.org/10.1007/s12520-020-01134-x.
14. Lucas HB, Silva HJA, Tasayco CMS, Munayco P, Faria JLB. Archaeological pottery from Nasca culture studied by Raman and Mössbauer spectroscopy combined with X-ray diffraction. Vib Spectrosc. 2018;97:140–5. https://doi.org/10.1016/j.vibspec.2018.06.010.
15. Maritan L, Nodari L, Mazzoli C, Milano A, Russo U. Influence of firing conditions on ceramic products: experimental study on clay rich in organic matter. Appl Clay Sci. 2006;31(1–2):1–15. https://doi.org/10.1016/j.clay.2005.08.007.
16. Forleo T, Giannossa LC, Laviano R, Mangone A. Exploring the raw materials and technological practice to obtain red and black surfaces of Apulian red figure pottery by Raman and SEM-EDS investigations. J Raman Spectrosc. 2022;53(4):810–9. https://doi.org/10.1002/jrs.6307.
17. Zhushchikhovskaya IS, Buravlev IY, Karpenko AA, Lazina AA, Fedorets AN. Red and black paints on prehistoric pottery of the southern Russian far east: an archaeometric study. Ceramics. 2023;6:1078–99. https://doi.org/10.3390/ceramics6020064.
18. Germinario C, Cultrone G, Bonis A, Izzo F, Langella A, Mercurio M, Nodari L, Vyhnal CR, Grifa C. μ-Raman spectroscopy as a useful tool for improving knowledge of ancient ceramic manufacturing technologies. Appl Clay Sci. 2024;253: 107347. https://doi.org/10.1016/j.clay.2024.107347.
19. Wagner FE, Kyek A. Mössbauer spectroscopy in archaeology: introduction and experimental considerations. Hyperfine Interact. 2004;154:5–33. https://doi.org/10.1023/B:HYPE.0000032112.94624.95.
20. Hunt A. The Oxford handbook of archaeological ceramic analysis. Oxford: Oxford University Press; 2017.
21. Akyuz S, Akyuz T, Basaran S, Bolcal C, Gulec A. Analysis of ancient potteries using FT-IR, micro-Raman and EDXRF spectrometry. Vib Spectrosc. 2008;48(2):276–80. https://doi.org/10.1016/j.vibspec.2008.02.011.
22. Eftekhari N, Holakooei P, Sayyadshahri H, Vaccaro C. Four shades of black: non-invasive scientific studies on the painted potteries from Shahr-i Sokhta, eastern Iran. J Archaeol Sci. 2018;22:100–7. https://doi.org/10.1016/j.jasrep.2018.09.012.
23. Olivares M, Zuluaga MC, Ortega LA, Murelaga X, Alonso-Olazabal A, Urteaga M, et al. Characterisation of fine wall and eggshell Roman pottery by Raman spectroscopy. J Raman Spectroscopy. 2010;41(11):1543–9. https://doi.org/10.1002/jrs.2748.

24. Wagner FE, Wagner U. Mössbauer spectra of clays and ceramics. Hyperfine Interact. 2004;154(1–4):35–82. https://doi.org/10.1023/B:HYPE.0000032113.42496.f2.
25. Lima DF, Toledo R, Martins A, Lima TO, Bertolino LC, Franco RWA. Fe^{III} in pottery: identifying firing temperature and ambiguity. Appl Clay Sci. 2020;190: 105581. https://doi.org/10.1016/j.clay.2020.105581.
26. Gütlich P, Bill E, Trautwein AX. Mössbauer spectroscopy and transition metal chemistry. In: Fundamentals and applications. Berlin: Springer; 2011. p. 73–135.
27. Nodari L, Maritan L, Mazzoli C, Russo U. Sandwich structures in the Etruscan-Padan type pottery. Appl Clay Sci. 2004;27(1–2):119–28. https://doi.org/10.1016/j.clay.2004.03.003.
28. Ricciardi P, Nodari L, Gualtieri S, De Simone D, Fabbri B, Russo U. Firing techniques of black slipped pottery from Nepal (12th-3rd century B.C.): the role of Mössbauer spectroscopy. J Cult Herit. 2008;9(3):261–8. https://doi.org/10.1016/j.culher.2007.12.003.
29. Maritan L, Mazzoli C, Nodari L, Russo U. Second Iron Age grey pottery from Este (northeastern Italy): study of provenance and technology. Appl Clay Sci. 2005;29(1):31–44. https://doi.org/10.1016/j.clay.2004.09.003.
30. Spataro M, Mommsen H, Villing A. Making pottery in the Nile Delta: ceramic provenance and technology at Naukratis, 6th–3rd centuries BC. Archaeol Anthropol Sci. 2019;11:1059–87. https://doi.org/10.1007/s12520-017-0584-4.
31. Marghussian AK, Coningham RAE, Fazeli H. Investigation of Neolithic pottery from Ebrahimabad in the central plateau of Iran, utilising chemical–mineralogical and microstructural analyses. J Archaeol Sci Rep. 2017;16:604–15. https://doi.org/10.1016/j.jasrep.2017.06.029.
32. Nodari L, Marcuz E, Maritan L, Mazzoli C, Russo U. Hematite nucleation and growth in the firing of carbonate-rich clay for pottery production. J Eur Ceram. 2007;27(16):4665–73. https://doi.org/10.1016/j.jeurceramsoc.2007.03.031.
33. Maschowski C, Kruspan P, Garra P, Arif AT, Trouvé G, Gieré R. Physicochemical and mineralogical characterization of biomass ash from different power plants in the upper Rhine region. Fuel (Lond). 2019;258: 116020. https://doi.org/10.1016/j.fuel.2019.116020.
34. Kim SK, Han MS, Nam SW, Jang S. Manufacturing characteristics of black burnished pottery from pungnaptoseong. Beakje J Conserv Sci. 2017;33(6):417–29. https://doi.org/10.12654/JCS.2017.33.6.02.
35. Brindley GW. Phyllosilicates. In: Mineralogy. Encyclopedia of earth science. Boston: Springer; 1981. p. 369–76.
36. Kim SK, Jang S, Lee CH. Production techniques of black burnished potteries from the Hanseong Period of the Baekje Kingdom (fourth to fifth century AD) in Ancient Korea. Archaeol Anthropol Sci. 2022;14(11):212. https://doi.org/10.1007/s12520-022-01675-3.
37. Trąbska J, Wesełucha-Birczyńska A, Zięba-Palus J, Runge MT. Black pained pottery, Kildehuse II, Odense country, Denmark. Spectrochim Acta Mol Biomol Spectrosoc. 2011;79(4):824–30. https://doi.org/10.1016/j.saa.2010.08.068.
38. Kokarneswaran M, Selvaraj P, Ashokan T, Perumal S, Sellappan P, Murugan KD, et al. Discovery of carbon nanotubes in sixth century BC potteries from Keeladi, India. Sci Rep. 2020;10(1):19786. https://doi.org/10.1038/s41598-020-76720-z.
39. Oancea AV, Bodi G, Nica V, Ursu LE, Drobota M, Cotofana C, Vasiliu AL, Simionescu BC, Olaru M. Multi-analytical characterization of Cucuteni pottery. J Eur Ceram. 2017;37(15):5079–98. https://doi.org/10.1016/j.jeurceramsoc.2017.07.018.
40. Liem NQ, Sagon G, Quang VX, Tan HV, Colomban P. Raman study of the microstructure, composition and processing of ancient Vietnamese (proto) porcelains and celadons (13–16th centuries). J Raman Spectrosc. 2000;31(10):933–42. https://doi.org/10.1002/1097-4555(200010)31:10%3c933::AID-JRS625%3e3.0.CO;2-0.
41. Legodi MA, de Waal D. Raman spectroscopic study of ancient South African domestic clay pottery. Spectrochim Acta A Mol Biomol Spectrosc. 2007;66(1):135–42. https://doi.org/10.1016/j.saa.2006.02.059.
42. Xu Y, An Z, Huang N, Zhao D. Analyzing the Shang-Western Zhou Dynasty pottery from the Jinsha Site with multi-technique method. Eur Phys J Plus. 2021;136(9):962. https://doi.org/10.1140/epjp/s13360-021-01952-5.
43. Colomban P, Treppoz F. Identification and differentiation of ancient and modern European porcelains by Raman macro and micro-spectroscopy. J Raman Spectrosc. 2001;32(2):93–102. https://doi.org/10.1002/jrs.678.
44. Liu WX. Modeling description and spectroscopic evidence of surface acid base properties of natural illites. Water Res. 2001;35(17):4111–25. https://doi.org/10.1016/s0043-1354(01)00156-7.
45. Colomban P, Maggetti M, d'Albis A. Non-invasive Raman identification of crystalline and glassy phases in a Sèvres Royal Factory soft paste porcelain plate. J Eur Ceram. 2018;38:5228–33.
46. Jadot E, Schiavon N, Manso M. The ceramics of Malpaís of Zacapu, Michoacán, Mexico, during the Early and Middle Postclassic periods (900–1459 AD): microchemical characterization of surface paintings. Spectrochim Acta B. 2016;119:10–6. https://doi.org/10.1016/j.sab.2016.03.002.
47. Keller R, Masch L, Pohl J, Schmidbauer E. Mineralogy, ^{57}Fe Mössbauer spectra and magnetization of chalcolithic pottery. Phys Chem Miner. 2005;32(3):165–74. https://doi.org/10.1007/s00269-005-0459-6.
48. Tschauner H, Wagner U. Pottery from a Chimú workshop studied by Mössbauer Spectroscopy. Hyperfine Interact. 2003;150(1–4):165–86. https://doi.org/10.1023/B:HYPE.0000007173.11484.7a.
49. Moon DH, Lee MS, Nam SW, Cho HG. A Study on magnetic properties and pole of the iron oxides in ancient Baekje black burnished pottery by Mössbauer spectroscopy. J Magn. 2020;25(4):496–502. https://doi.org/10.4283/JMAG.2020.25.4.496.
50. Dormann JL, Viart N, Rehspringer JL, Ezzir A, Niznansky D. Magnetic properties of Fe2O3 particles prepared by sol-gel method. Hyperfine Interact. 1998;112(1/4):89–92. https://doi.org/10.1023/A:1011088611227.
51. Kündig W, Bömmel H, Constabaris G, Lindquist RH. Some properties of supported small α−Fe_2O_3 particles determined with the Mössbauer effect. Phys Rev. 1966;142(2):327–33. https://doi.org/10.1103/PhysRev.142.327.
52. Munayco P, Scorzelli RB. Characterization of the firing conditions of archaeological Marajoara pottery by Mössbauer spectroscopy and X-ray diffraction. Hyperfine Interact. 2013;222(S1):69–75. https://doi.org/10.1007/s10751-012-0656-x.
53. Heller-Kallai L, Rozenson I. The use of Mössbauer spectroscopy of iron in clay mineralogy. Phys Chem Miner. 1981;7(5):223–38. https://doi.org/10.1007/BF00311893.
54. Wang F, Yang J, Shi L, Shen J. Manufacturing technique analysis of Early Harappan painted pottery from the Jhang Bahatar Site, Pakistan, by using a multi-analytical approach. J Archaeol Sci. 2024;53: 104369. https://doi.org/10.1016/j.jasrep.2023.104369.
55. Lima LKS, Silva KR, Menezes RR, Santana LNL, Lira HL. Microstructural characteristics, properties, synthesis and applications of mullite: a review. Cerâmica. 2022;68:126–42. https://doi.org/10.1590/0366-69132022683853184.
56. Jastrzębska I, Szczerba J, Stoch P, Błachowski A, Ruebenbauer K, Prorok R, Śnieżek E. Crystal structure and Mössbauer study of $FeAl_2O_4$. Nukleonika. 2015;60(1):47–9. https://doi.org/10.1515/nuka-2015-0012.
57. Jastrzębska I, Szczerba J, Stoch P, Błachowski A, Stoch P. Structure and microstructure evolution of hercynite spinel ($Fe^{2+}Al_2O_4$) after annealing treatment. Eur J Chem. 2017;29(1):63–72. https://doi.org/10.1127/ejm/2017/0029-2579.
58. Gong C, Lu Z, Shen J, Zhang Q, Cao H, Liu G, Wu Z, Zhou K, Xia Y, Liu M. Mössbauer study of the black-glazed Jian bowl in the Song Dynasty. Int J Appl Ceram Technol. 2023;20(6):3795–802. https://doi.org/10.1111/ijac.14439.
59. Nasab HV, Nikzad M, Jayez M, Hashemi M, Knapp Z, Sykes N, Khalili MZ, Moghaddam HI, Nasab FB, Olszewski DI. Komishan cave: a mesolithic and later settlement on the southeastern Shore of the Caspian Sea. Iran Anc Near East Stud. 2020;57:97–125. https://doi.org/10.2143/ANES.57.0.3288614.
60. Maritan L. Archaeometric study of Etruscan-Padan type pottery from the Veneto region: petrographic mineralogical and geochemical-physical characterization. Eur J Miner. 2004;16(2):297–307. https://doi.org/10.1127/0935-1221/2004/0016-0297.

Publisher's Note